Prediction of Li_nCd compounds with unusual stoichiometry and valence states

Han Liu,[1] Jianyun Wang,[1] Quan Li,[1,*] and Changfeng Chen[2,†]

[1]*State Key Lab of Superhard Materials and International Center for Computational Method and Software, College of Physics, Jilin University, Changchun 130012, China*

[2]*Department of Physics and Astronomy, University of Nevada, Las Vegas, Nevada 89154, USA*

(Received 28 September 2020; accepted 24 November 2020; published 14 December 2020)

Cadmium (Cd) and its compounds are a family of materials exhibiting diverse physical and chemical properties that find wide-ranging applications in many science and technology fields. In all known Cd compounds, Cd ions behave like a typical d-block element, donating electrons and adopting positive (+2 or +1) charge states. To explore the possibility of forming compounds with Cd in negative charge states, would greatly expand this material family and enrich understanding of the associated physical and chemical properties and the underlying mechanisms. Here, we report on an exemplary case study via a systematic search and examination of Li-Cd binary compounds over a wide range of stoichiometry. We have employed an unbiased crystal structure search method in conjunction with first-principles energetic calculations to predict viable crystal structures under ambient and high-pressure conditions. Our investigations have identified a series of stable Li_nCd compounds with an unusually wide range ($n = 1$–6) of stoichiometry at both ambient and high pressures. Strikingly, our results reveal that Cd attracts electrons from Li in forming a rich variety of bonding configurations with the Cd ions adopting a range of negative charge states, producing highly tunable structural and electronic properties. Moreover, calculated elastic parameters show that the mechanical properties of LiCd compound can be enhanced considerably over those of Li and Cd metals and other Li-Cd binary compounds. We analyze the charge transfer from Li to Cd and the resulting electron distribution patterns and find a significant and variable amount of partial occupation of the Cd-5p states in this traditional d-block element. The present findings provide insights into fundamental knowledge and practical processes in valence state control for tuning transitions from d- to p-block behaviors via a proper choice of compound formation and application of high pressure. The results expand conventional definition and understanding of charge states in the compound formation and enrich structure-property relations that have broad implications for Li-rich binary compounds.

DOI: 10.1103/PhysRevMaterials.4.123604

I. INTRODUCTION

As a member of the d-block [1] metals with the valence-electron configuration of $4d^{10}5s^2$, cadmium (Cd) can form compounds with a wide range of physical and chemical properties that find extensive applications in, for example, electrical conductors [2–4], batteries [5–7], the manufacture of alloys [8,9], and pigments and plastics [10,11]. Cadmium is widely used in the field of electroplating [12,13], particularly as one of the primary corrosion protection agents for aircraft steel structures [14]. These functional properties are largely determined by the arrangement of valence electrons in the outermost shell of cadmium [15]. In general, cadmium possesses fully filled d-electron shells in the elemental or common oxidation states. The most common oxidation state of Cd is +2, but it also exhibits +1 state in some compounds [16,17].

The degree of oxidation of an atom in a chemical compound is related to the atom's electronegativity [18] that determines its ability to gain or lose electrons. The higher the electronegativity the stronger the atom's ability of attracting electron. Due to the 4d-block contraction, the electronegativity (Pauling scale) of cadmium is 1.69, which is even slightly higher than that of Zn (1.65), contrary to the general rule that electronegativity decreases on passing from top to bottom along the same group of elements in the Periodic table. If cadmium could be made to gain electrons from a less electronegative element in forming stable stoichiometric compounds, its 5p states would be partially occupied, resulting in a valence electron configuration of $4d^{10}5s^25p^n$, which is isoelectronic with the main-group elements of In ($n = 1$), Sn ($n = 2$), Sb ($n = 3$), and so on. As a result, the oxidation state of cadmium would be negative, which will inevitably modulate the associated physical and chemical properties. Such an scenario is of considerable theoretical and experimental interest and is expected to stimulate exploration for potential expanded applications.

Alkali metals possess the highest electropositivity [19,20], thus they are expected to be the most suitable candidates to provide electrons to Cd in adopting negative charge states and forming various compounds with unusual stoichiometries. Among the alkali metals, lithium (Li) is a prominent case that has wide applications, for example, in battery production [21–25], ceramics [26,27], glass [28–30], lubricant [31,32], and refrigeration liquid [33], among others.

*liquan777@calypso.cn
†chen@physics.unlv.edu

 ©2020 American Physical Society

We therefore have chosen Li as a promising candidate as a reactant in the chemical reaction with Cd, with the expectation that the resulting compounds would have Cd in negative valence states that are sensitive to the internal bonding configurations and also to the external conditions like pressure. Such Li-Cd compounds should exhibit a wide range of structural, electronic, and mechanical properties derived from the unusual combination of Li and Cd in their flexible bonding states. The variation of charge and bonding states would likely produce a variety of chemical stoichiometries, and pressure is expected to act as an important tool to modulate the structure and functional performance, which would help examine and expand viable Cd-containing compounds. In particular, pressure is known to be a highly versatile and effective tool to help overcome activation energy barriers of chemical reactions [34], rearrange atomic orbital energy levels [35], cause structural phase transitions [36,37], and change electronic properties [38]. Recent years have seen a number of unexpected stoichiometric compounds with extraordinary properties [39–44] have been theoretically designed and experimentally synthesized, which are not accessible at ambient pressure. It is thus worthwhile to search and examine thermodynamically stable Li-Cd compounds in an effort to enlarge and enrich a wide range of useful materials for understanding and technological development.

II. COMPUTATIONAL METHODS

Alkali metals are known to provide electrons to a *d*-block element, e.g., Au [45], making it behave as a *p*-block element. In this work, we systematically explore the crystal structures of Li_nCd ($n = 1$–6) compounds using the CALYPSO structure search method [46–49] in conjunction with first-principles energetic calculations. This method has been successfully applied to predict structures, ranging from elemental to binary and ternary compounds [50–57], which served as the basis for probing intriguing structural, electronic and transport properties [58–65]. In this work, we have adopted the same approach to identify viable compounds through systematic structure searches and then examine their properties that exhibit various behaviors under different chemical and physical environments. Our structure searches of Li_nCd ($n = 1$–6) were performed at 0, 20, 50, and 100 GPa with simulation cell sizes of 1, 2 and 4 formula units (f.u.). The *ab initio* structural relaxations and electronic band-structure calculations were carried out in the framework of density functional theory as implemented in the Vienna *ab initio* simulation package (VASP) code [66]. The exchange-correlation potential [67] is described by using the generalized gradient approximation (GGA) within the Perdew-Burke-Ernzerhof (PBE) framework. The all-electron projector augmented-wave method (PAW) [68] is performed to describe the electron-ion interaction, where the $1s^2 2s^1$ and $4d^{10} 5s^2$ are treated as the valence states for Li and Cd atoms, respectively. The cutoff energy of 600 eV and appropriate Monkhorst-Pack k meshes with spacing of $2\pi \times 0.03$ Å^{-1} were used to ensure that all the enthalpy calculations were converged well. We performed calculations to obtain phonon dispersions by using the direct supercell method [69] as provided in the PHONOPY code [70] to check dynamic stability of predicted compounds. A Bader charge analysis has been carried out to examine charge transfer [71], which is obtained by dividing the space into Bader basins around each atom based on the fixed points of the charge density. By integrating the charges in each basin, the total charge associated with each atom is obtained. We calculated the elastic constants of Li-Cd compounds by using the strain-stress method, and calculated the bulk modulus and shear modulus using the Voigt-Reuss-Hill (VRH) averaging scheme, adopting a kinetic energy cutoff of 800 eV to achieve proper computational accuracy.

III. RESULTS AND DISCUSSIONS

Our structural search yields many thermodynamically stable or metastable Li-Cd structures at ambient and high-pressure conditions. The enthalpy of formation per atom

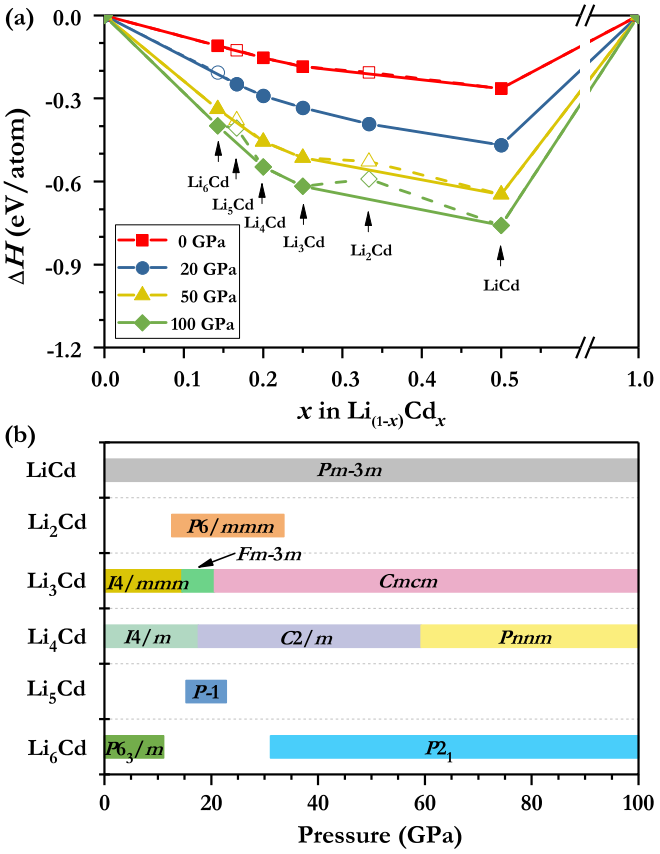

FIG. 1. Stability of the Li-Cd compounds. (a) Calculated enthalpy of formation per atom of the Li-Cd compounds with respect to decomposition into elemental Li and Cd solid phases. The energetically stable phases at each pressure are shown by solid symbols, which are connected by the convex hull (solid lines). Dotted lines that directly connect data points are visual guides. The $Im-3m$ (0–1 GPa), $Fm-3m$ (1–40 GPa), $I-43d$ (40–65 GPa), $Aba2$-40 (65–80 GPa), and $Pbca$ (80–100 GPa) structures of elemental Li solids, and $P6_3/mmc$ symmetry (0–100 GPa) of elemental Cd solid were used as the reference materials to calculate the formation enthalpies [72]. (b) Pressure-composition phase diagram of stable Li-Cd binary compounds.

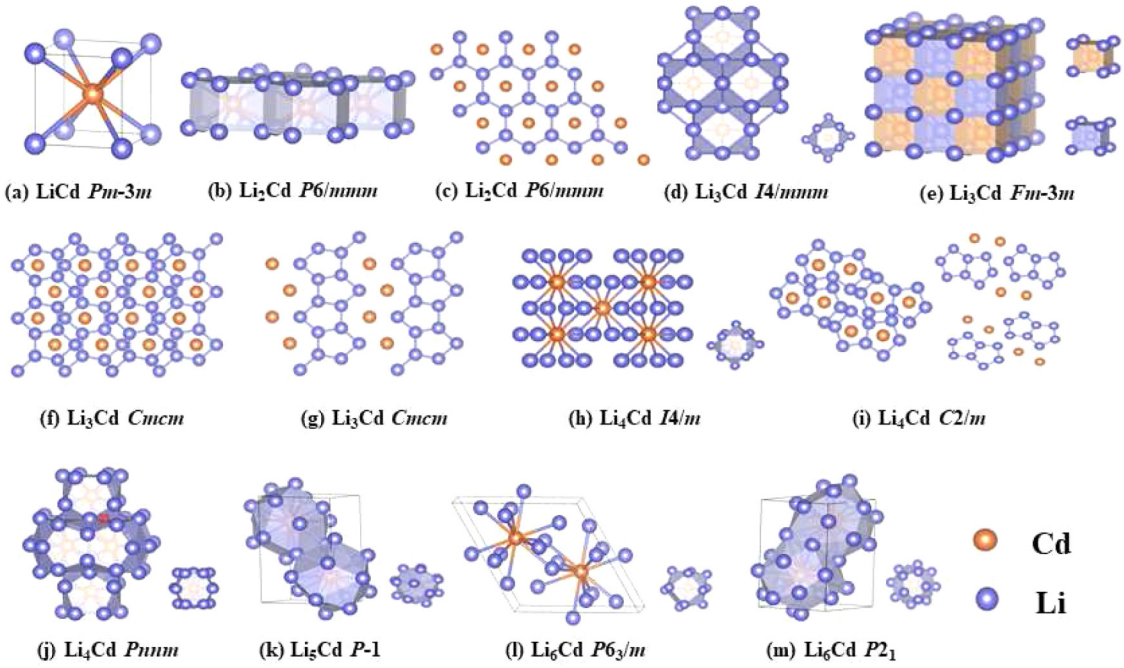

FIG. 2. Crystal structures of viable Li-Cd compounds. (a) LiCd in the $Pm{-}3m$ structure. (b) Li_2Cd in the $P6/mmm$ structure. (c) Li_2Cd in the $P6/mmm$ structure containing a graphene-like Li layer. (d) Li_3Cd in the $I4/mmm$ structure. (e) Li_3Cd in the $Fm{-}3m$ structure. (f) The double layered structures of Li_3Cd in the *Cmcm* structure. (g) The single layered Li_3Cd in the *Cmcm* structure. (h) Li_4Cd in the $I4/m$ structure. (i) The layered Li_4Cd in the $C2/m$ structure. (j) Li_4Cd in the *Pnnm* structure. (k) Li_5Cd in the P-1 structure. (l) Li_6Cd in the $P6_3/m$ structure. (m) Li_6Cd in the $P2_1$ structure.

of Li_nCd was calculated by using the following equation: $\Delta H(\mathrm{Li}_n\mathrm{Cd}) = [H(\mathrm{Li}_n\mathrm{Cd})\text{-}nH(\mathrm{Li})\text{-}H(\mathrm{Cd})]/(n+1)$, where H and ΔH are the calculated enthalpy per chemical unit for each compound and the enthalpy of formation per atom, respectively. The formation enthalpy at different pressures and pressure-composition phase diagram for Li-Cd systems with various chemical stoichiometries lie on the convex hull (Fig. 1). These Li-Cd structures sitting right on the convex hull are stable against decomposition, and thus are expected to be viable for experimental synthesis, while the structures above the convex hull are thermodynamically metastable, which may also appear in synthesized products under proper conditions. The CALYPSO method combined with first-principles energetic calculations are capable to perform structural design of alloy structures [50] and reveal the tendency of decomposition [73] if they are energetically favorable. Without the consideration of temperature effect, our results show that the ordered structures have advantages in thermodynamic stability at ambient pressure with formation enthalpies of -0.1 to -0.3 eV/atom. The pressure effect further stabilizes the Li-Cd binary compounds with superior formation enthalpy up to -0.8 eV/atom. It should be pointed out that the configuration entropy of alloy at high-temperature conditions will play a vital role to enhance its thermodynamic stability, however, the studies of temperature effect are beyond the scope of this work. At ambient conditions, the formation enthalpy results of the $Pm{-}3m$ LiCd, $I4/mmm$ Li_3Cd, $I4/m$ Li_4Cd, and $P6_3/m$ Li_6Cd are located on the convex hull, while those of $P6/mmm$ Li_2Cd and P-1 Li_5Cd are slightly above the convex hull. The crystal structures of the thermodynamically stable stoichiometries are shown in Fig. 2. LiCd has a primitive cubic CsCl-type structure [Fig. 2(a)] with a two-atom basis, which is one of the most common and simplest phases in ionic compounds. In this structure, each Cd (Li) atom has eight adjacent Li (Cd) atoms and six adjacent Cd atoms, forming a simple cube, while the Li (Cd) atoms lie in the voids at the center of the cubes. Note that we have employed several pseudopotentials to examine the reliability of the exchange-correlation functionals. The theoretical equilibrium lattice parameters for LiCd with the PBE-GGA, the strongly constrained and appropriately normed (SCAN) meta-GGA [74,75], Tao-Perdew-Staroverov-Scuseria meta-generalized-gradient-approximation (TPSS-MGGA) [76], and Ceperly-Alder local density approximation (CA-LDA) functional [77] are 3.326, 3.260, 3.295, and 3.190 Å, respectively, which are all in excellent agreement with the experimental result of 3.32 Å [78]. We employed the PBE-GGA for the results and discussion reported below due to this high degree of consistency in the produced lattice parameters. Li_3Cd adopts a close-packed Al_3Ti-type structure with the space group of $I4/mmm$ at ambient pressure [Fig. 2(d)]. Here, Cd atoms locate at the centers and are enclosed by the face-sharing Li tetradecahedrons, while Li atoms form polymeric frameworks involving tunnels along the a axis. Li_4Cd and Li_6Cd are crystalized into a tetragonal structure with $I4/m$ symmetry [Fig. 2(h)] and a hexagonal lattice with $P6_3/m$ symmetry [Fig. 2(l)], respectively. In both cases, each Cd atom is surrounded by twelve Li atoms. Calculated phonon dispersions, which are shown in Fig. 3, reveal no imaginary vibrational modes for the identified phases, indicating that these phases are dynamically

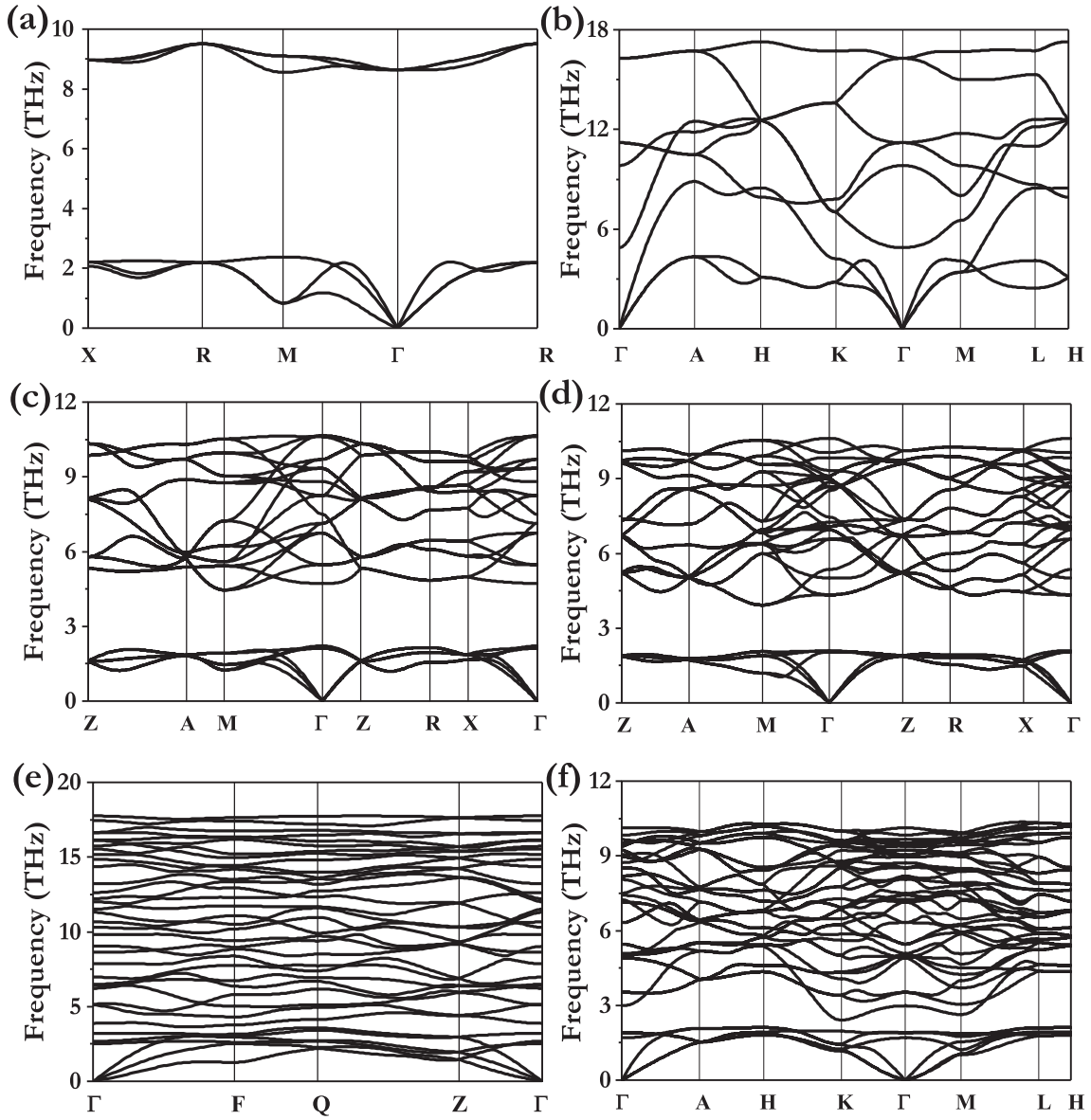

FIG. 3. Phonon dispersions of LiCd with $Pm-3m$ symmetry at 0 GPa (a), Li_2Cd with $P6/mmm$ symmetry at 20 GPa (b), Li_3Cd with $I4/mmm$ symmetry at 0 GPa (c), Li_4Cd with $I4/m$ symmetry at 0 GPa (d), Li_5Cd with P-1 symmetry at 20 GPa (e), and Li_6Cd with $P6_3/m$ symmetry at 0 GPa (f).

stable in their corresponding pressure ranges. Further details on the calculated structural parameters and Wyckoff positions for all the identified Li_nCd compounds are summarized in Table I.

At high pressures, Li_3Cd, Li_4Cd and Li_6Cd compounds undergo a series of structural phase transformations, while $Pm-3m$ LiCd is thermodynamically stable throughout the entire pressure range from 0 to 100 GPa. Li_3Cd undergoes two structural phase transitions, first from $I4/mmm$ to $Fm-3m$ then to $Cmcm$ phase with the transition pressures of 14.5 and 20.6 GPa, respectively. $Fm-3m$ Li_3Cd can be considered as a superlattice of $Pm-3m$ LiCd with half the Cd atoms replaced by Li atoms [Fig. 2(e)]. For $Cmcm$ Li_3Cd [Fig. 2(g)], Cd atoms form zigzag chains with Cd-Cd distance of 2.974 Å, and Li atoms form connected and twisted five-membered rings. Li_4Cd transforms from $I4/m$ to $C2/m$ structure at 17.6 GPa, then to $Pnnm$ structure at 59.3 GPa. $C2/m$ Li_4Cd is a monoclinic structure with interlocking five-membered rings, separated by Cd atoms [Fig. 2(i)]. For $Pnnm$ Li_4Cd, a noteworthy feature of this structure is that there are fifteen Li atoms surrounding each Cd atoms [Fig. 2(j)]. Li_6Cd with $P6_3/m$ symmetry becomes metastable at 11.1 GPa, and then transforms into a thermodynamically stable structure with monoclinic $P2_1$ symmetry above 31.1 GPa. Moreover, two pressure-stabilized Li-Cd compounds with exotic stoichiometry of Li_2Cd and Li_5Cd are predicted here. Li_2Cd has a MgB_2-type structure with space group $P6/mmm$ [Fig. 2(b)], consisting of face-sharing Cd-Li octahedrons. In this structure, Li atoms in the ab plane form graphene-like layered structures [Fig. 2(c)] with intercalated Cd atoms. Li_5Cd is predicted to be stable in P-1 symmetry with Cd atoms encapsulated in Li_{15} pseudocages [Fig. 2(k)].

TABLE I. The calculated lattice parameters (in angstroms) and atomic positions for the selected stable Li_nCd structures.

	Space group	Pressure (GPa)	Lattice parameters	Atom	Site	Atomic positions x	y	z
LiCd	$Pm-3m$	0	$a=b=c=3.3259$	Li	1*a*	0.0000	0.0000	0.0000
			$\alpha=\beta=\gamma=90.00$	Cd	1*b*	0.5000	0.5000	0.5000
Li_2Cd	$P6/mmm$	20	$a=b=4.0443$	Li	2*a*	0.3333	0.6667	0.5000
			$c=2.6958$	Cd	1*a*	0.0000	1.0000	1.0000
			$\alpha=\beta=90.00$					
			$\gamma=120.00$					
Li_3Cd	$I4/mmm$	0	$a=b=4.3343$	Li	2*b*	0.5000	0.5000	0.0000
			$c=7.8652$	Li	4*d*	0.5000	1.0000	0.2500
			$\alpha=\beta=\gamma=90.00$	Cd	2*a*	1.0000	1.0000	0.0000
	$Fm-3m$	20	$a=b=c=5.8294$	Li	4*b*	0.5000	1.0000	1.0000
			$\alpha=\beta=\gamma=90.00$	Li	8*c*	0.2500	0.7500	0.7500
				Cd	4*a*	0.5000	0.5000	1.0000
	$Cmcm$	100	$a=3.6034$	Li	4*c*	0.5000	0.7059	0.2500
			$b=7.6213$	Li	8*f*	0.5000	0.8841	0.5503
			$c=4.5184$	Cd	4*c*	0.0000	0.0910	0.7500
			$\alpha=\beta=\gamma=90.00$					
Li_4Cd	$I4/m$	0	$a=b=6.6190$	Li	8*h*	0.3971	0.7942	1.0000
			$c=4.2732$	Cd	2*a*	0.5000	0.5000	0.5000
			$\alpha=\beta=\gamma=90.00$					
	$C2/m$	50	$a=12.3495$	Li	4*i*	0.6904	1.0000	0.0522
			$b=3.7432$	Li	4*i*	0.6051	1.0000	0.2645
			$c=7.5841$	Li	4*i*	0.1652	1.0000	0.2268
			$\alpha=\gamma=90.00$	Li	4*i*	0.8512	0.5000	0.2741
			$\beta=148.33$	Cd	4*i*	0.9689	1.0000	0.6441
	$Pnnm$	100	$a=6.4058$	Li	4*g*	0.5297	0.8628	0.0000
			$b=6.4062$	Li	4*g*	0.3630	0.9682	0.5000
			$c=3.6093$	Li	4*g*	0.9025	0.9036	0.5000
			$\alpha=\beta=\gamma=90.00$	Li	4*g*	0.8022	0.8043	1.0000
				Cd	4*g*	0.6486	0.6499	0.5000
Li_5Cd	P-1	20	a=4.4821	Li	2*i*	0.1207	0.8138	0.0421
			$b=4.4796$	Li	2*i*	0.0490	0.4515	0.2507
			$c=7.3485$	Li	2*i*	0.4715	0.3017	0.1073
			$\alpha=92.91$	Li	2*i*	0.3157	0.6223	0.5429
			$\beta=92.85$	Li	2*i*	0.8031	0.9722	0.6076
			$\gamma=105.84$	Cd	2*i*	0.6545	0.8446	0.2499
Li_6Cd	$P6_3/m$	0	a=b=7.9167	Li	6*h*	0.0576	0.8113	0.7500
			$c=4.9210$	Li	6*h*	0.0971	0.6125	0.2500
			$\alpha=\beta=90.00$	Cd	2*d*	0.3333	0.6667	0.7500
			$\gamma=120.00$					
	$P2_1$	50	a=5.0318	Li	4*a*	1.0000	0.0080	0.3377
			$b=7.0362$	Li	4*a*	1.0000	0.2308	0.1730
			$c=6.9982$	Li	8*b*	0.7678	0.0861	0.6005
			$\alpha=\beta=\gamma=90.00$	Li	8*b*	0.8102	0.3436	0.4486
				Cd	4*a*	0.5000	0.1382	0.2878

We have calculated the projected density of states (PDOS) to examine the electronic properties of these predicted Li-Cd compounds. The theoretical PDOS of Li_3Cd and Li_6Cd are selected as representative results, as shown in Figs. 4 and 5, respectively. At ambient pressure, the Fermi level of $I4/mmm$ Li_3Cd is dominated by Cd 5*p*, Li 2*s* and Li 2*p* states (Fig. 4), indicating charge transfer from Li 2*s* and 2*p* to Cd 5*p* states. Here, we construct an idealized model of Li_0In at 0 GPa, in which all Li atoms were removed from their lattice sites and all Cd atoms were replaced by indium (In) atoms. From the PDOS for Li_3Cd and Li_0In, the direct comparison between Cd 5*p* states and In 5*p* states [Fig. 4(d)] shows that the Cd 5*p* states distribute in the similar energy range as those of In 5*p* states. These results demonstrate that Cd atom in Li_3Cd behaves like and therefore should be regarded as a *p*-block element, which stems from the bonding configuration modulation at the various chemical stoichiometry.

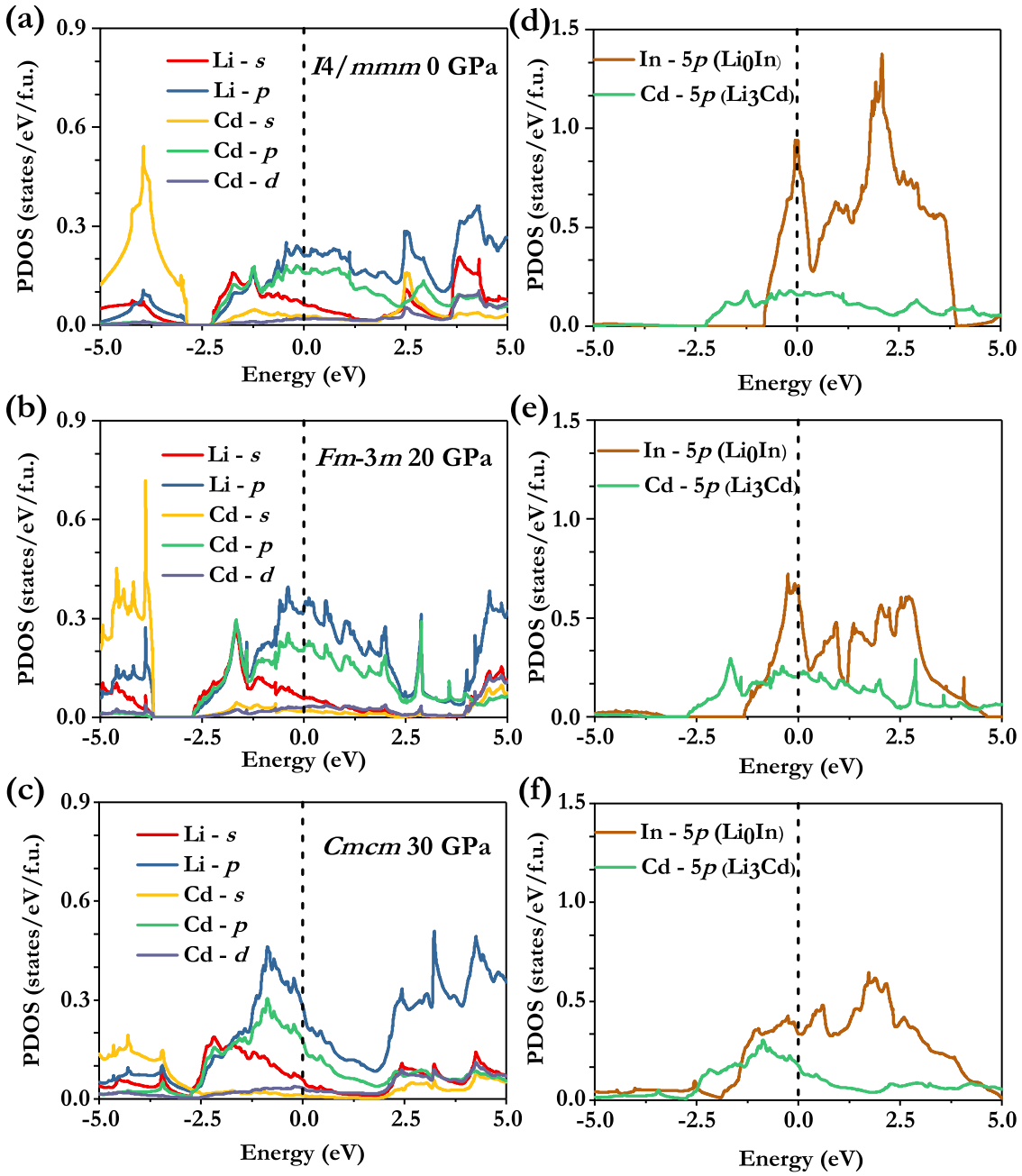

FIG. 4. The PDOS of Li_3Cd in (a) $I4/mmm$ structure at 0 GPa, (b) $Fm{-}3m$ structure at 20 GPa, and (c) *Cmcm* structure at 30 GPa. The occupation of the $5p$ state of Cd in Li_3Cd within the (d) $I4/mmm$ at 0 GPa, (e) $Fm{-}3m$ structure at 20 GPa, and (f) *Cmcm* structure at 30 GPa are compared with the result of the $5p$ states for In as modeled by Li_0In.

To examine the pressure effects on the behaviors of electron transfer, we have examined the PDOS of $Fm{-}3m$ Li_3Cd at 20 and *Cmcm* Li_3Cd at 30 GPa, as shown in Figs. 4(b) and 4(c), respectively. Similar to the results at ambient pressures, the theoretical PDOS results reveal a noticeable Cd $5p$ component below the Fermi level for the high-pressure phases of Li_3Cd. The integrated Cd $5p$ states below the Fermi level of Li_3Cd at rising pressure increases monotonically, demonstrating that rising pressure enhances electron transfer from Li to Cd. We also constructed two similar model systems of Li_0In at 20 GPa and 30 GPa by removing all Li atoms from their lattice sites and replacing all Cd atoms with In atoms. It is noted that the distributing characteristics of the Cd $5p$ states in both $Fm{-}3m$ and *Cmcm* phases at high pressures are quite similar to the In $5p$ states for Li_0In [Figs. 4(e)–4(f)]. We show in Fig. 5 the PDOS results of $P6_3/m$ phase at 0 GPa and $P2_1$ structure at 50 GPa for Li_6Cd. The calculated results are in accordance with the conclusion as in the case of Li_3Cd. Based on the results of $P6_3/m$ structure at 0 GPa and $P2_1$ structure at 50 GPa for Li_6Cd, we have structured a series of model systems, in which Li atoms are removed one by one from the structures. The calculated PDOS of Li_xCd ($x = 6$–0) are presented in Figs. 6(a) and 6(b). Decreasing Li content results in a significantly decreasing Cd $5p$ component below

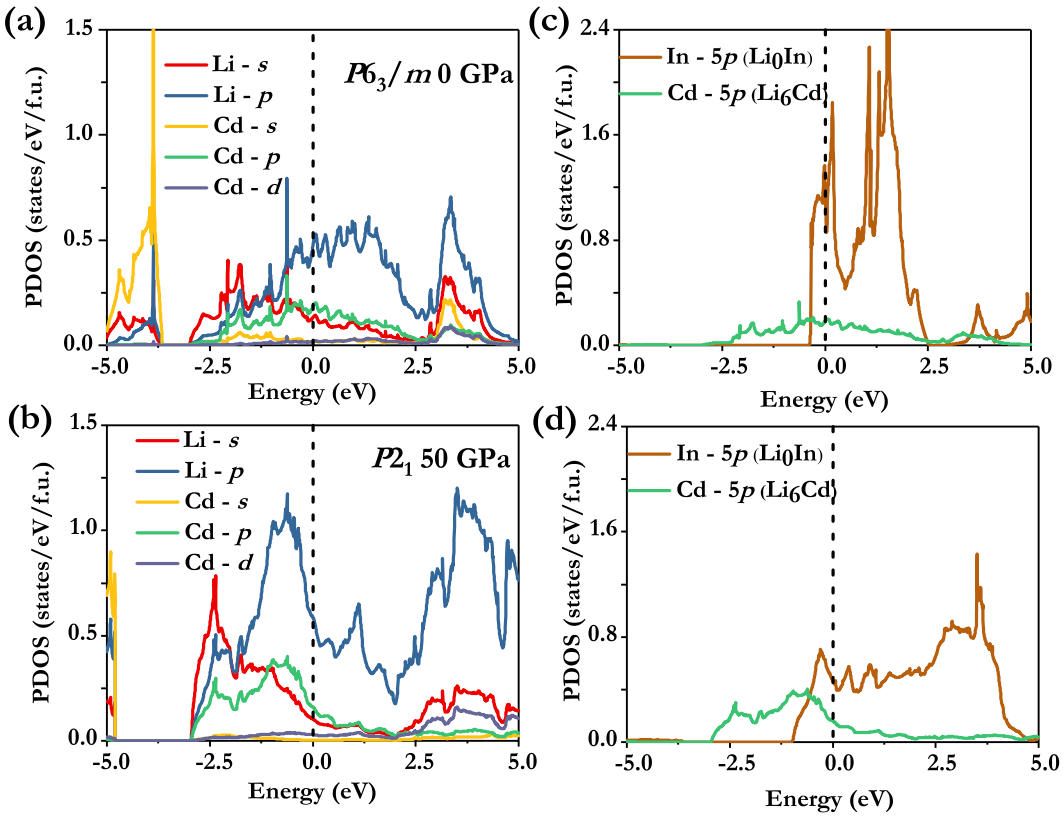

FIG. 5. The PDOS of Li_6Cd in the (a) $P6_3/m$ structure at 0 GPa and (b) $P2_1$ structure at 50 GPa. The occupation of the 5p state of Cd in Li_6Cd within the (c) $P6_3/m$ at 0 GPa and (d) $P2_1$ structure at 50 GPa are compared with the result of the 5p states for In as modeled by Li_0In.

the Fermi level, illustrating that the Li-Cd charge transfer can be efficiently adjusted by controlling the Li composition in these compounds. We also performed a Bader charge analysis, which provides a description of electron transfer between Li and Cd, to quantify the amount of charge belonging to each atom for different stable chemical stoichiometries. Here, we have selected 20 GPa as a reference pressure point where the chemical stoichiometries for Li_nCd ($n = 1$–5) are all thermodynamically stable. The calculated charge amounts on Cd are −0.77, −1.54, −2.30, −3.00, and −3.76, for LiCd, Li_2Cd, Li_3Cd, Li_4Cd, and Li_5Cd, respectively, indicating that the negative oxidation state of Cd may be −1, −2, or −3. Our results reveal that the charge states of Cd increase almost linearly with progressively higher concentration of Li, indicating a systematic charge transfer pattern in Li-Cd compounds with variable chemical stoichiometry. Our results show that Cd effectively attracts electrons from Li either modulated by the changing chemical stoichiometry, or driven by applied pressure to form $4d^{10}5s^25p^n$ electronic configurations, thereby behaving as a 5p element. The electronic configurations of negative charge states in Cd, isoelectronic with the main-group elements of In, Sn, or Sb, leads to similar physical and chemical proprieties with those of the above elements, which expand related functional application and prospects.

To elucidate the mechanism underlying the intriguing phenomenon of Cd behaving like a 5p element in the unusual Li_nCd compounds, we analyze the pressure effect on the atomic orbital energy levels for Li and Cd atoms. The calculated results are shown in Fig. 7. It is seen that at ambient pressure the 2s orbit of Li is about 1.7 eV lower than the 5p orbit of Cd, whereas the 2p orbit of Li is slightly higher than the 5p orbit of Cd by 0.3 eV. These relative energetic arrangements promote a physical environment that promotes charge transfer from the Li to Cd atoms in these Li-Cd compounds, making Cd act as a p-block element despite its typical d-block element designation based on its position in the Periodic Table and its behaviors in previously reported studies. Note that pressure affects the atomic orbital energy levels of Li and Cd elements and cause various degrees of charge response in different compounds and at changing pressures. With the pressure increasing, the orbital energy levels of Li 2s and Li 2p rise much faster than Cd 5p, and thus the Li 2s orbital level overpasses the Cd 5p level at pressures around 51 GPa. As a result, the orbital energy levels of Li 2s and Li 2p become higher than the Cd 5p level, leading to a more pronounced charge transfer from Li to Cd at high pressures. This character indicates that pressure acts as an effective driving force for charge transfer in the Li-Cd compounds and promotes Cd to act as a 5p element when it is alloyed with Li. Overall, the electron transfer from Li to Cd orbital occurs at both ambient and high pressures, which is favorable for Cd to behave as a p element in forming these unusual compounds.

Metallic light-element compounds with H-rich or Li-rich stoichiometries have attracted considerable attention in searching for room-temperature superconductivity, which

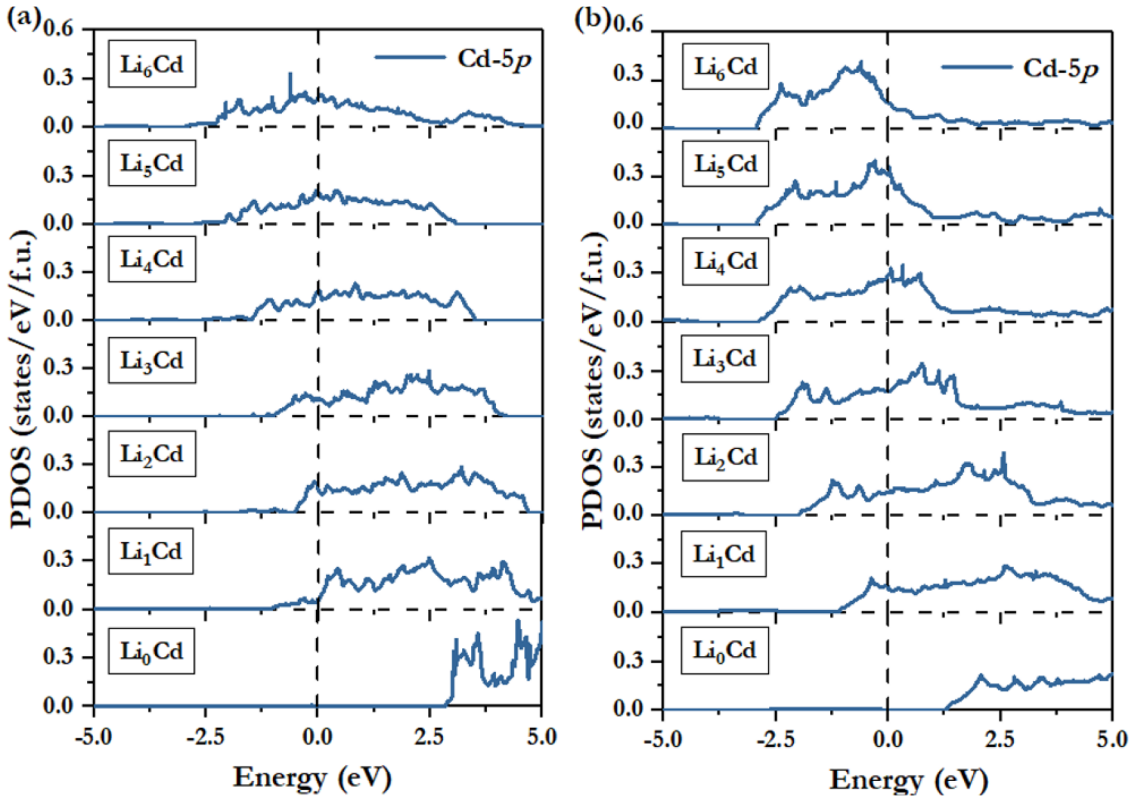

FIG. 6. The PDOS of Cd in Li_xCd ($x = 6$–0) with the (a) $P6_3/m$ structure at 0 GPa and (b) $P2_1$ structure at 50 GPa, in which Li atoms are removed one by one from the Li_6Cd structure.

is an important topic in condensed matter physics since the prediction and discovery of superconductivity in H-S [54,79–81], La-H [56,82–85], Li-S-H [86], Li-Mg-H [87], and Li-P [42] systems. It is noted that the simultaneous combination of high electronic density near the Fermi level and low phonon frequencies (especially below10 THz) emerges in the current predicted Li-Cd binary compounds, which has been suggested as favorable to enhance electron pairing and electron-phonon coupling, essential to superconducting performance in conventional superconductors. Therefore there is a high possibility that the current Li-rich compounds are superconducting, which may stimulate extensive experimental research on the preparation and measurement of these materials.

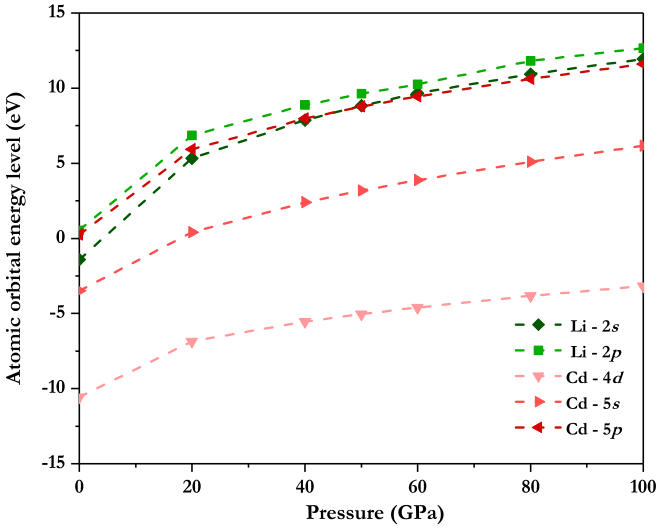

FIG. 7. Atomic orbital energy levels for Li and Cd atoms as a function of pressure. Pressure effect is modeled by putting elements in a face-centered cubic (fcc) He matrix. An fcc supercell containing 108 He atoms ($3 \times 3 \times 3$) is used, in which one He atom is replaced by the atom being examined. As the pressure increases, Li $2s$ and $2p$ orbital energy levels rise faster than the Cd $5p$ level.

Mechanical properties characterized by various elastic moduli have great impacts on many potential applications of Li-Cd compounds. To assess key mechanical properties, we have calculated bulk modulus (B), shear modulus (G), and Young's modulus (E) for the identified viable Li-Cd compounds at ambient pressure, and the obtained results are summarized in Table II. It is seen that the calculated bulk

TABLE II. Calculated bulk modulus (B), Shear modulus (G), Young's modulus (E), and density (ρ) for Cd, Li_nCd, and Li.

Phases	B (GPa)	G (GPa)	E (GPa)	ρ (g/cm^3)
Cd	38.75	9.11	25.35	8.65
LiCd	31.00	15.68	40.26	5.39
Li_3Cd	22.41	8.89	23.56	2.99
Li_4Cd	20.52	10.15	26.15	2.49
Li_6Cd	18.22	8.32	21.67	1.92
Li	13.69	6.07	15.85	0.53

modulus of Li_nCd increases monotonously with the increasing Cd content, including the two end members, i.e., the Li and Cd metals. This result indicates that the ability of these materials to resist volume changes gets stronger when an increasing proportion of Cd is introduced into the Li-Cd compounds. This phenomenon can be understood primarily based on the density of these compounds (see the calculated data listed in Table II), which provides a good measure of the ability for a material to resist compression. Meanwhile, the shear modulus and Young's modulus of these Li_nCd compounds also exhibit an upward trend with increasing of Cd content, reaching peak values for LiCd. It is fascinating to note that both of these moduli decrease considerably for Cd metal compared to the results for LiCd; however, these reduced elastic moduli for Cd metal still remain higher than the values for all other members of this Li-Cd family of compounds studied in this work. This phenomenon indicates that the electron transfer in the Li-Cd compound with a Li:Cd ratio of 1:1 produces the optimal bonding environment in LiCd that generates the strongest bonding network with the highest capability of resistance to shear and tensile deformations among this series of compounds. Meanwhile, from the results in Fig. 1, it is also seen that LiCd exhibits high structural stability, remaining in the same $Pm-3m$ structure in the entire pressure range of 0 GPa up to 100 GPa without any pressure induced structural transformation, which showcases the superior bonding strength in this structural configuration. Combining these shear modulus and Young's modulus results with the high bulk modulus, LiCd stands out as the most prominent member of the Li-Cd series of compounds in terms of mechanical performance characters. The robust stability of LiCd also bodes well for its potential synthesis and application under versatile loading conditions.

IV. SUMMARY

In summary, we have performed extensive and systematic structural searches to identify viable crystal phases of Li-Cd compounds under ambient and high pressures by using an advanced unbiased structure prediction method in conjunction with first-principles energetic calculations. Our results show that Li and Cd can form a series of stable compounds with unusual stoichiometry at both ambient and high-pressure conditions. Of the six Li_nCd (n=1-6) compounds identified, four are stable at ambient pressure, while the other two are stabilized at rising pressures. Three of these compounds ($n = 3$, 4, and 6) undergo pressure induced structural phase transformations, two ($n = 2$ and 5) are stable only in a relatively small pressure range, while one ($n = 1$) remains robust in the entire pressure range of 0–100 GPa examined in this study.

We have carried out a detailed analysis of the electronic structures of these compounds at ambient conditions, and the results show that the Cd $5p$ states make a pronounced contribution to the states below the Fermi level. The pressure induced the volume reduction and interaction enhancement play crucial yet various roles in the modulation of the charge transfer from Li to Cd in different members of this family of compounds. A Bader charge analysis reveals a large amount of charge transfer from Li to Cd facilitated by both the unusual chemical stoichiometry and pressure effects. This result highlights a couple of highly unusual aspects of the Li-Cd compounds: (1) Cd normally loses electrons in forming most known compounds, e.g., cadmium oxides, but here it gains electrons in forming compounds with Li, an alkali element with lower electronegativity; (2) Cd is normally regarded as a typical d-block element; but here Cd adopts an unusual $4d^{10}5s^25p^n$ electron configuration with variable partial occupation of the $5p$ states in various Li-Cd compounds and, therefore, acts as a p-block element. The appearance of the negative oxidation states in Cd makes it act as a main-group element with similar physical and chemical proprieties as those of the isoelectronic In, Sn, or Sb, thus expanding related functional application and prospects. These results reveal various type and range of Cd-containing compounds in terms of viable stoichiometry, charge state, and bonding configuration, which may help expand both material forms and physical properties of these compounds for improved understanding of a large family of unusual compounds and their potential applications. For the Li-Cd compounds with fixed Li compositions, the higher the pressure, the more charge is transferred; meanwhile, at a certain pressure point, the more Li components, the more charge is transferred. Among the identified Li-Cd compounds, the bulk modulus, shear modulus and Young's modulus of the viable phases exhibit an upward trend with increasing Cd content, although the latter two quantities see a sizable reduction in going from LiCd compound to Cd metal. The increasing density caused by the rising Cd content in the Li_nCd serious of compounds and the two end members of Li and Cd metals is likely most responsible for the monotonously rising bulk modulus, while the steadily rise of the shear and Young's moduli throughout the series but an appreciable drop in going to Cd metal indicates more subtle effect of charge transfer and bonding network strengthening that seem to be optimized in LiCd with a 1:1 Li:Cd ratio. Coupled with its versatile and robust structural stability, LiCd stands out as a prominent member among Li-Cd compounds for excellent mechanical characters that are important to many applications.

The present findings expand considerably the understanding of Cd-containing compounds, especially the unusual rich variety of stoichiometry and negative charge states. The prolific scenarios of variable degrees of partial occupation of the $5p$ states of Cd in the Li_6Cd compounds make fascinating cases of turning a typical d-block element, i.e., Cd, into a versatile and robust p-block element in its oxidation and bonding behaviors that have great impacts on generating diverse material properties.

ACKNOWLEDGMENTS

This research was supported by the National Key Research and Development Program of China under Grant No. 2018YFA0703404, the Natural Science Foundation of China under Grants No. 11622432, 11534003, and Program for JLU Science and Technology Innovative Research Team (JLUSTIRT). We utilized computing facilities at the High-Performance Computing Center of Jilin University and Tianhe2-JK at the Beijing Computational Science Research Center.

H.L. and J.W. contributed equally to this work.

[1] E. C. Constable, Evolution and understanding of the d-block elements in the periodic table, Dalton. Trans. **48**, 9408 (2019).

[2] R. S. Crandall, Electrical conduction in n-type cadmium sulfide at low temperatures, Phys. Rev. **169**, 577 (1967).

[3] J. D. Klein, R. D. Herrick, D. Palmer, M. J. Sailor, C. J. Brumlik, and C. R. Martin, Electrochemical fabrication of cadmium chalcogenide microdiode arrays, Chem. Mater. **5**, 902 (1993).

[4] D. Ravinder, S. S. Rao, and P. Shalini, Room temperature electric properties of cadmium-substituted nickel ferrites, Mater. Lett. **57**, 4040 (2003).

[5] D. C. Reynolds, G. Leies, L. L. Antes, and R. E. Marburger, Photovoltaic effect in cadmium sulfide, Phys. Rev. **96**, 533 (1954).

[6] D. Liu and P. V. Kamat, Photoelectrochemical behavior of thin cadmium selenide and coupled titania/cadmium selenide semiconductor films, J. Phys. Chem. **97**, 10769 (1993).

[7] L. N. Kulikova, M. A. Volgin, and A. L. Lévov, Cadmium composite materials for lithium batteries: Synthesis and investigation of electrochemical behavior, Russ. J. Electrochem. **41**, 620 (2005).

[8] M. Hirabayashi and S. Ogawa, Crystal structures and phase transitions of the gold-rich gold-cadmium alloy, Acta. Metall. **9**, 264 (1961).

[9] H. Morrow, *Cadmium and Cadmium Alloys, Kirk-Othmer Encyclopedia of Chemical Technology* 5th ed. (John Wiley & Sons, New York, 2010).

[10] W. G. Huckle, G. F. Swigert, and S. E. Wiberley, Cadmium pigments. structure and composition, Ind. Chem. Prod. Res. Dev. **5**, 362 (1966).

[11] J. Paulus and U. Knuutinen, Cadmium colours: Compositionand properties, Appl. Phys. A **79**, 397 (2004).

[12] G. Hodes, J. Manassen, S. Neagu, D. Cahen, and Y. Mirovsky, Electroplated cadmium chalcogenide layers: Characterization and use in photoelectrochemical solar cells, Thin. Sol. Films. **90**, 433 (1982).

[13] A. M. El-hakm, Electroplating of cadmium from acidic bromide baths, J. Appl. Electrochem. **14**, 587 (1984).

[14] E. Huttunen-Saarivirta, H. Korpiniemi, V.-T. Kuokkala, and H. Paajanen, Corrosion of cadmium plating by runway de-icing chemicals: Study of surface phenomena and comparison of corrosion tests, Surf. Coat. Tech. **232**, 101 (2013).

[15] L. Pauling, *The Nature of the Chemical Bond* (Cornell University Press, New York, 1960).

[16] S. Riedel and M. Kaupp, The highest oxidation states of the transition metal elements, Coordin. Chem. Rev. **253**, 606 (2009).

[17] B. Zhou, M. S. Denning, T. A. D. Chapman, J. E. McGrady, and J. M. Goicoechea, $[Pb_9CdCdPb_9]^{6-}$: A zintl cluster anion with an unsupported cadmium-cadmium bond, Chem. Commun. **46**, 7221 (2009).

[18] R. G. Parr and R. G. Pearson, Absolute hardness: Companion parameter to absolute electronegativity, J. Am. Chem. Soc. **105**, 7512 (1983).

[19] Y. Ma, M. Eremets, A. R. Oganov, Y. Xie, I. Trojan, S. Medvedev, A. O. Lyakhov, M. Valle, and V. Prakapenka, Transparent dense sodium, Nature (London) **458**, 182 (2009).

[20] J. Lv, Y. Wang, L. Zhu, and Y. Ma, Predicted Novel High-Pressure Phases of Lithium, Phys. Rev. Lett. **106**, 015503 (2011).

[21] C. K. Chan, H. Peng, G. Liu, K. McIlwrath, X. F. Zhang, R. A. Huggins, and Y. Cui, High-performance lithium battery anodes using silicon nanowires, Nat. Nanotechnol. **3**, 31 (2008).

[22] M. S. Whittingham, Lithium batteries and cathode materials, Chem. Rev. **104**, 4271 (2004).

[23] B. Scrosati and J. Garche, Lithium batteries: Status, prospects and future, J. Power. Sources **195**, 2419 (2010).

[24] E. Yoo, J. Kim, E. Hosono, H. Zhou, T. Kudo, and I. Honma, Large reversible li storage of graphene nanosheet families for use in rechargeable lithium ion batteries, Nano Lett. **8**, 2277 (2008).

[25] K. S. Kang, Y. S. Meng, J. Breger, C. P. Grey, and G. Ceder, Electrodes with high power and high capacity for rechargeable lithium batteries, Science **311**, 977 (2006).

[26] H. Aono, High Li^+ conducting ceramics, Acc. Chem. Res. **27**, 265 (1994).

[27] E. Hollenstein, M. Davis, D. Damjanovic, and N. Setter, Piezoelectric properties of Li- and Ta-modified $(K_{0.5}Na_{0.5})NbO_3$ Ceramics, Appl. Phys. Lett. **87**, 182905 (2005).

[28] J. Fu, Superionic conductivity of glass-ceramics in the system Li_2O-Al_2O_3-TiO_2-P_2O_5, Solid. State. Ion. **96**, 195 (1997).

[29] J. Fu, Fast Li^+ ion conducting glass-ceramics in the system Li_2O-Al_2O_3-GeO_2-P_2O_5, Solid. State. Ion. **104**, 191 (1997).

[30] T. Zhang, N. Imanishi, S. Hasegawa, A. Hirano, J. Xie, Y. Takeda, O. Yamamoto, and N. Sammes, Li/polymer electrolyte/water stable lithium-conducting glass ceramics composite for lithium-air secondary batteries with aqueous electrolyte, J. Electrochem. Soc. **155**, A965 (2008).

[31] Z. Song, M. Fan, Y. Liang, F. Zhou, and W. Liu, Lithium-based ionic liquids: *In situ*-formed lubricant additive only by blending, Tribol. Lett. **49**, 127 (2013).

[32] Z. Song, M. Fan, Y. Liang, F. Zhou, and W. Liu, Lithium-based ionic liquids as novel lubricant additives for multiply alkylated cyclopentanes (MACs), Friction **1**, 222 (2013).

[33] B. Narvóez-Romo, M. Chhay, E. W. Zavaleta-Aguilar, and J. R. Simões-Moreira, A critical review of heat and mass transfer correlations for LiBr-H_2O and NH_3-H_2O absorption refrigeration machines using falling liquid film technology, Appl. Therm. Eng. **123**, 1079 (2017).

[34] E. Zurek, R. Hoffmann, N. W. Ashcroft, A. R. Oganov, and A. O. Lyakhov, A little bit of lithium does a lot for hydrogen, Proc. Natl. Acad. Sci. USA **106**, 17640 (2009).

[35] M. Miao, Caesium in high oxidation states and as a *p*-block element, Nat. Chem. **5**, 846 (2013).

[36] W. Wang, A. Li, G. Xu, P. Wang, Y. Liu, and L. Wang, Synthesis of polycrystalline diamond compact with selenium: Discovery of a new se-c compound, Chin. Phys. Lett. **37**, 058101 (2020).

[37] C. Pei, Y. Xia, J. Wu, Y. Zhao, L. Gao, T. Ying, B. Gao, N. Li, W. Yang, D. Zhang, H. Gou, Y. Chen, H. Hosono, G. Li, and Y. Qi, Pressure-induced topological and structural phase transitions in an antiferromagnetic topological insulator, Chin. Phys. Lett. **37**, 066401 (2020).

[38] R. S. McWilliams, D. K. Spaulding, J. H. Eggert, P. M. Celliers, D. G. Hicks, R. F. Smith, G. W. Collins, and R. J. Jeanloz, Phase transformations and metallization of magnesium oxide at high pressure and temperature, Science **338**, 1330 (2012).

[39] J. Botana and M. Miao, Pressure-stabilized lithium caesides with caesium anions beyond the -1 state, Nat. Commun. **5**, 4861 (2014).

[40] F. Peng, Y. Yao, H. Liu, and Y. Ma, Crystalline LiN_5 predicted from first-principles as a possible high-energy material, J. Phys. Chem. Lett. **6**, 2363 (2015).

[41] J. Lin, S. Zhang, W. Guan, G. Yang, and Y. Ma, Gold with +4 and +6 oxidation states in AuF_4 and AuF_6, J. Am. Chem. Soc. **140**, 9545 (2018).

[42] Z. Zhao, S. Zhang, T. Yu, H. Xu, A. Bergara, and G. Yang, Predicted Pressure-Induced Superconducting Transition in Electride Li_6P, Phys. Rev. Lett. **122**, 097002 (2019).

[43] F. Peng, M. Miao, H. Wang, Q. Li, and Y. Ma, Predicted lithium-boron compounds under high pressure, J. Am. Chem. Soc. **134**, 18599 (2012).

[44] J. Lin, Z. Zhao, C. Liu, J. Zhang, X. Du, G. Yang, and Y. Ma, IrF_8 molecular crystal under high pressure, J. Am. Chem. Soc. **141**, 5409 (2019).

[45] G. Yang, Y. Wang, F. Peng, A. Bergara, and Y. Ma, Gold as a 6*p*-element in dense lithium aurides, J. Am. Chem. Soc. **138**, 4046 (2016).

[46] Y. Wang, J. Lv, L. Zhu, and Y. Ma, Crystal structure prediction via particle-swarm optimization, Phys. Rev. B **82**, 094116 (2010).

[47] Y. Wang, J. Lv, L. Zhu, and Y. Ma, CALYPSO: A method for crystal structure prediction, Comput. Phys. Commun. **183**, 2063 (2012).

[48] B. Gao, P. Gao, S. Lu, J. Lv, Y. Wang, and Y. Ma, Interface structure prediction via CALYPSO method, Sci. Bull. **64**, 301 (2019).

[49] Y. Wang, M. Miao, J. Lv, L. Zhu, K. Yin, H. Liu, and Y. Ma, An effective structure prediction method for layered materials based on 2D particle swarm optimization algorithm, J. Chem. Phys. **137**, 224108 (2012).

[50] L. Zhu, H. Wang, Y. Wang, J. Lv, Y. Ma, Q. Cui, Y. Ma, and G. Zou, Substitutional Alloy of Bi and Te at High Pressure, Phys. Rev. Lett. **106**, 145501 (2011).

[51] H. Wang, J. S. Tse, K. Tanaka, T. Iitaka, and Y. Ma, Superconductive sodalite-like clathrate calcium hydride at high pressures, Proc. Natl. Acad. Sci. USA **109**, 6463 (2012).

[52] Q. Li, D. Zhou, W. Zheng, Y. Ma, and C. Chen, Global Structural Optimization of Tungsten Borides, Phys. Rev. Lett. **110**, 136403 (2013).

[53] L. Zhu, H. Liu, C. J. Pickard, G. Zou, and Y. Ma, Reactions of xenon with iron and nickel are predicted in the earth's inner core, Nat. Chem. **6**, 644 (2014).

[54] Y. Li, J. Hao, H. Liu, Y. Li, and Y. Ma, The metallization and superconductivity of dense hydrogen sulfide, J. Chem. Phys. **140**, 174712 (2014).

[55] M. Zhang, H. Liu, Q. Li, B. Gao, Y. Wang, H. Li, C. Chen, and Y. Ma, Superhard BC_3 in Cubic Diamond Structure, Phys. Rev. Lett. **114**, 015502 (2015).

[56] F. Peng, Y. Sun, C. J. Pickard, R. J. Needs, Q. Wu, and Y. Ma, Hydrogen Clathrate Structures in Rare Earth Hydrides at High Pressures: Possible Route to Room-Temperature Superconductivity, Phys. Rev. Lett. **119**, 107001 (2017).

[57] W. Gong, C. Liu, X. Song, Q. Li, Y. Ma, and C. Chen, Unravelling the Structure and Strength of the Highest Boride of Tungsten $WB_{4.2}$, Phys. Rev. B **100**, 220102(R) (2019).

[58] Q. Li, D. Zhou, W. Zheng, Y. Ma, and C. Chen, Anomalous Stress Response of Ultrahard WB_n Compounds, Phys. Rev. Lett. **115**, 185502 (2015).

[59] C. Lu, Q. Li, Y. Ma, and C. Chen, Extraordinary Indentation Strain Stiffening Produces Superhard Tungsten Nitrides, Phys. Rev. Lett. **119**, 115503 (2017).

[60] C. Lu and C. Chen, High-pressure evolution of crystal bonding structures and properties of FeOOH, J. Phys. Chem. Lett. **9**, 2181 (2018).

[61] J. Zhang, J. Lv, H. Li, X. Feng, C. Lu, S. A. T. Redfern, H. Liu, C. Chen, and Y. Ma, Rare Helium-Bearing Compound FeO_2He Stabilized at Deep-Earth Conditions, Phys. Rev. Lett. **121**, 255703 (2018).

[62] X. Song, K. Yin, Y. Wang, A. Hermann, H. Liu, J. Lv, Q. Li, C. Chen, and Y. Ma, Exotic hydrogen bonding in compressed ammonia hydrides, J. Phys. Chem. Lett. **10**, 2761 (2019).

[63] S. Deng, X. Song, X. Shao, Q. Li, Y. Xie, C. Chen, and Y. Ma, First-principles study of high-pressure phase stability and superconductivity of Bi_4I_4, Phys. Rev. B **100**, 224108 (2019).

[64] C. Liu, X. Song, Q. Li, Y. Ma, and C. Chen, Smooth Flow in Diamond: Atomistic Ductility and Electronic Conductivity, Phys. Rev. Lett. **123**, 195504 (2019).

[65] C. Liu, X. Song, Q. Li, Y. Ma, and C. Chen, Superconductivity in Compression-Shear Deformed Diamond, Phys. Rev. Lett. **124**, 147001 (2020).

[66] K. Momma and F. Izumi, VESTA 3 for three-dimensional visualization of crystal, volumetric and morphology data, J. Appl. Crystallogr. **44**, 1272 (2011).

[67] J. P. Perdew, K. Burke, and M. Ernzerhof, Generalized Gradient Approximation Made Simple, Phys. Rev. Lett. **77**, 3865 (1996).

[68] P. E. Blóchl, Phys. Rev. B: Condens. Matter. **50**, 17953 (1994).

[69] K. Parlinski, Z. Li, and Y. Kawazoe, First-Principles Determination of the Soft Mode in Cubic ZrO_2, Phys. Rev. Lett. **78**, 4063 (1997).

[70] A. Togo, F. Oba, and I. Tanaka, First-principles calculations of the ferroelastic transition between rutile-type and $CaCl_2$-type SiO_2 at high pressures, Phys. Rev. B **78**, 134106 (2008).

[71] W. Tang, E. Sanville, and G. A. Henkelman, Grid-based bader analysis algorithm without lattice bias, J. Phys.- Condens. Mat. **21**, 084204 (2009).

[72] T. Kenichi, Structural study of Zn and Cd to ultrahigh pressures, Phys. Rev. B **56**, 5170 (1997).

[73] X. Yang, H. Li, H. Liu, H. Wang, Y. Yao, Y. Xie, Pressure-induced decomposition of binary lanthanum intermetallic compounds, Phys. Rev. B **101**, 184103 (2020).

[74] J. Sun, R. Adrienn, and P. P. John, Strongly Constrained and Appropriately Normed Semilocal Density Functional, Phys. Rev. Lett. **115**, 036402 (2015).

[75] Y. Zhang, A. K. Daniil, J. Yang, T. Chen, T. D. Stephen, A. S. Rafael, A. L. M. Maguel, H. Peng, C. Gerbrand, P. P. John, and J. Sun, Efficient first-principles prediction of solid ttability: Towards chemical accuracy, npj Comput. Mater. **4**, 9 (2018).

[76] J. Sun, M. Marsman, G. Csonka, A. Ruzsinszky, P. Hao, Y.-S. Kim., G. Kresse, and J. P. Perdew, Self-consistent meta-generalized gradient approximation within the projector-augmented-wave method, Phys. Rev. B **84**, 035117 (2011).

[77] D. M. Ceperley and B. J. Alder, Ground State of the Electron Gas by a Stochastic Method, Phys. Rev. Lett. **45**, 566 (1980).

[78] W. B. Pearson, *A Handbook of Lattice Spacings and Structures of Metals and Alloys* (Pergamon Press, Oxford, 1964).

[79] D. Duan, Y. Liu, F. Tian, D. Li, X. Huang, Z. Zhao, H. Yu, B. Liu, W. Tian, and T. Cui, Pressure-induced metallization of

dense $(H_2S)_2H_2$ with High-Tc superconductivity, Sci. Rep. **4**, 6968 (2014).

[80] A. Drozdov, M. Erements, I. Troyan, V. Ksenofontov, and S. Shylin, Conventional superconductivity at 203 kelvin at high pressures in the sulfur hydride system, Nature (London) **525**, 73 (2015).

[81] C. Liu, H. Zhai, Y. Sun, W. Gong, Y. Yan, Q. Li, and W. Zheng, Strain-induced modulations of electronic structure and electron-phonon coupling in dense H_3S, Phys. Chem. Chem. Phys. **20**, 5952 (2018).

[82] H. Liu, I. Naumov, R. Hoffmann, N. Ashcroft, and R. Hemeley, Potential High-Tc superconducting lanthanum and yttrium hydrides at high pressure, Proc. Natl. Acad. Sci. USA **114**, 6990 (2017).

[83] Z. Geballe, H. Liu, A. Mishra, M. Ahart, M. Somayazulu, Y. Meng, M. Baldini, and R. Hemley, Synthesis and stability of lanthanum superhydrides, Angew. Chem. Int. Edit. **57**, 688 (2018).

[84] A. Drozdov, P. Kong, V. Minkov, S. Besedin, M. Kuzovnikov, S. Mozaffari, L. Balicas, F. Balakirev, D. Graf, V. Prakapenka, E. Greenberg, D. Knyazev, M. Tkacz, and M. Eremets, Superconductivity at 250 K in lanthanum hydride under high pressures, Nature (London) **569**, 528 (2019).

[85] M. Somayazulu, M. Ahart, A. K. Mishra, Z. M. Geballe, M. Baldini, Y. Meng, V. V. Struzhkin, and R. J. Hemley, Evidence for Superconductivity above 260 K in Lanthanum Superhydride at Megabar Pressures, Phys. Rev. Lett. **122**, 027001 (2019).

[86] P. Zhang, Y. Sun, X. Li, J. Lv, and H. Liu, Structure and superconductivity in compressed Li-Si-H compounds: Density functional theory calculations, Phys. Rev. B **102**, 184103 (2020).

[87] Y. Sun, J. Lv, Y. Xie, H. Liu, and Y. Ma, Route to a Superconducting Phase above Room Temperature in Electron-Doped Hydride Compounds under High Pressure, Phys. Rev. Lett. **123**, 097001 (2019).